International Journal of Mechanical Sciences 131–132 (2017) 744–752

Contents lists available at ScienceDirect

International Journal of Mechanical Sciences

journal homepage: www.elsevier.com/locate/ijmecsci

Comparison of plane-stress, generalized-plane-strain and 3D FEM elastic–plastic analyses of thick-walled cylinders subjected to radial thermal gradient

S.M. Kamal [a], U.S. Dixit [b,*], A. Roy [c], Q. Liu [c], Vadim V. Silberschmidt [c]

[a] Department of Mechanical Engineering, Tezpur University, Napaam, Tezpur 784 028, India
[b] Department of Mechanical Engineering, Indian Institute of Technology Guwahati, Guwahati 781 039, India
[c] Wolfson School of Mechanical, Electrical and Manufacturing Engineering, Loughborough University, Loughborough LE11 3TU, UK

ARTICLE INFO

Keywords:
Thick-walled cylinder
Elastic–plastic
Plane stress
Generalized plane strain
Three-dimensional finite element method
Thermal stress

ABSTRACT

In many industrial applications, thick-walled cylindrical components are subjected to high pressure and/or temperature. During the operation the cylinder wall may undergo elastic–plastic deformation. This paper presents plane-stress and plane-strain thermo-elastic–plastic stress analyses of thick-walled cylinders subjected to a radial thermal gradient. A three-dimensional finite element method (3D FEM) analysis of the thermo-elastic–plastic stresses in thick-walled cylinder is also carried out. The 3D FEM results are compared with the analytical plane stress and the generalized plane strain analyses in order to study the validity of these models on the basis of length to wall-thickness ratio of cylinders. The plane stress and generalized plane strain analyses are based on the Tresca yield criterion and associated flow rule. The strain hardening behavior of the material of the cylinder is taken into account. It is observed that for the length to wall thickness ratio of more than 6, the generalized plane strain analysis can provide sufficiently accurate results. Similarly, for the length to wall thickness ratio of less than 0.5, plane stress analysis can be used. When the length to wall thickness ratio is more than 0.5 but less than 6, a three-dimensional analysis is needed.

1. Introduction

The thick-walled cylinders subjected to pressures and temperatures find several applications, e.g., in chemical industries and nuclear power plants. In most of the cases, the design attempts to keep the stresses in the cylinders within elastic limits. However, it is always better to carry out an elastic–plastic analysis in order to get an idea about safety in case of untoward situations. Moreover, in an autofrettage process, the plastic deformation is deliberately produced to induce compressive stresses in the inner side of the cylinder. There are also examples where plastic deformation is permitted by design. Thus, the elastic–plastic analysis of the thick-walled cylinders is an attractive research area.

Elastic–plastic deformation of thick-walled cylinders due to internal pressure loading is well recognized and has been investigated by many researchers. Many analytical solutions are available for stress, strains and displacement fields during the elastic–plastic deformation of cylinders. An early analysis of elastic–plastic deformation in thick tubes was carried out by Hill et al. [1] assuming non-hardening material, Tresca yield criterion and plane strain condition. Gao [2] developed a closed form analytical solution for the elastic–plastic stress, strain and displacements of an internally pressurized thick-walled cylinders under plane stress condition using Hencky's deformation theory and von Mises yield criterion. Durban [3], Gao [4], and Bonn and Haupt [5] investigated large elastic–plastic deformations of thick-walled cylindrical tube under internal pressure. An analytical solution for stress, strain and displacements in thick cylinder subjected to internal pressure was developed by Gao [6] using strain gradient plasticity theory. An analytical solution for elastic–plastic stresses considering the Bauschinger effect and Tresca yield criterion in thick-walled cylindrical vessel made of elastic linear-hardening material was given by Darijani et al. [7].

The classical solution for thermo-elastic stresses in thick-walled cylindrical bodies under steady state temperature distribution due to temperature gradient is well known. However, only a few papers treat the thermo-elastic–plastic analysis of thick-walled cylinders analytically. Bland [8] carried out an elastic–plastic analysis of thick-walled tubes of work hardening material subjected to internal and external pressures with outer and inner surfaces maintained at different temperatures. He considered that yielding took place only on the inner side of

* Corresponding author.
E-mail addresses: uday@iitg.ac.in, usd1008@yahoo.com (U.S. Dixit).

http://dx.doi.org/10.1016/j.ijmecsci.2017.07.034
Received 4 September 2016; Received in revised form 2 June 2017; Accepted 20 July 2017
Available online 10 August 2017

Nomenclature

a	inner radius of cylinder
b	outer radius of cylinder
c, d, e, f	interface radii
E	Young's modulus of elasticity
K	hardening coefficient
n	strain hardening exponent
r	radius of cylinder
T_a	temperature at the inner wall of cylinder
T_b	temperature at the outer wall of cylinder
u	radial displacement
α	coefficient of thermal expansion
ε_r	total radial strain
ε_θ	total hoop strain
ε_0	constant axial strain
ε_r^e, ε_θ^e, ε_z^e	elastic radial, hoop and axial strain
ε_r^p, ε_θ^p, ε_z^p	plastic radial, hoop and axial strain
$\varepsilon_{\text{eq}}^p$	equivalent plastic strain
ν	Poisson's ratio
σ_r	radial stress
σ_θ	hoop stress
σ_z	axial stress
σ_{eq}	equivalent stress
σ_Y	yield stress

the cylinder leading to the formation of an inner plastic zone. Wong and Simionescu [9] developed an elastic–plastic analytical model of thick-walled tube subjected to internal heating and pressure assuming small displacements, plane strain condition and the yield criterion of Tresca without strain hardening. They did not consider the case in which there are outer and inner plastic zones with an intermediate elastic zone. The thermo-elastic–plastic deformation of tubes with inner plastic and outer elastic zones due to internal heat generation was investigated by Orçan and Eraslan [10] considering the temperature-dependent mechanical and thermal properties. Sadeghian and Toussi [11] carried out an axisymmetric thermo-elastic–plastic stress analysis in cylindrical vessels made of functionally graded material. The stress analysis of a functionally graded thick-walled hyperelastic spherical vessel subjected to internal and external pressure was carried out by Anani and Rahimi [12], albeit without considering thermal stresses. Some papers in the literature deal with the thermo-elastic–plastic analysis of solid cylinders and spherical vessels. Orçan [13] carried out a thermo-elastic–plastic analysis of elastic-perfectly plastic cylindrical rod with uniform internal heat generation for generalized plane strain condition based on Tresca yield criterion. He considered the case of two plastic zones separated by an elastic zone. Cowper [14], Johnson and Mellor [15], and Darijani et al. [16] analyzed the elastic–plastic stresses in thick-walled hollow sphere under steady state radial temperature gradient. In a recent paper, Zare and Darijani [17] studied elastic–plastic stresses in a thick-walled cylinder rotating at a very large angular velocity.

In general, a thick-walled cylinder may undergo simultaneous plastic deformations emanating from both inner and outer walls under the condition of high thermal gradient. This case was analyzed by Kamal and Dixit [18,19] for a hollow disk and cylinder assuming plane stress and generalized plane strain conditions, respectively. The analyses are based on Tresca yield criterion and its associated flow rule. The effect of strain hardening was considered in the plane stress model [18]. However, the generalized plane strain model [19] did not include the strain hardening, although the theoretical results matched well with the experiments [20].

In this work, the generalized plane strain model of Kamal and Dixit [19] is extended to incorporate the effect of strain-hardening. The strain-hardening during plastic deformation is assumed to follow Ludwik's hardening law. The plane stress and generalized plane strain models cannot predict the dimension-range in which the respective assumptions are justified. Hence, a three-dimensional finite element method (3D FEM) analysis is carried out in order to define the applicability of the analytical models. A criterion based on the length to wall thickness ratio of the cylinders is developed to assess the validity of the plane stress and generalized plane strain assumptions. During the analysis, it is assumed that the maximum temperature induced in the cylinder is well below the recrystallization temperature of the material. Hence, it is appropriate to treat the mechanical and thermal properties of the material as temperature-independent.

2. Problem definition

A thick-walled cylinder with inner radius a and outer radius b is considered. The inner wall is subjected to a temperature T_a and the outer wall is subjected to a temperature T_b such that $T_b > T_a$. The thermo-elastic–plastic stress analyses of a short cylinder (hollow circular disk) using the assumption of plane stress ($\sigma_z = 0$) incorporating strain hardening was carried out in [18]. Another analytical model based on a generalized plane-strain condition ($\varepsilon_z =$ constant) applicable for long cylinders is available in [19]. However, the generalized plane-strain model did not include the effect of strain hardening. In the present work, the thermo-elastic–plastic stress analysis in the cylinder under the generalized plane-strain assumption is presented incorporating the strain hardening in Section 3. The material is assumed to follow the Ludwik's hardening law given by [21]:

$$\sigma_{\text{eq}} = \sigma_Y + K\left(\varepsilon_{\text{eq}}^p\right)^n, \tag{1}$$

where σ_Y is the yield stress in uniaxial tension or compression, σ_{eq} ($>\sigma_Y$) is the equivalent stress, $\varepsilon_{\text{eq}}^p$ is the equivalent plastic strain, K is the hardening coefficient and n is the strain hardening exponent. A steady-state temperature distribution in the cylinder under a radial temperature difference ($T_b - T_a$) is given by [22]:

$$T = T_a + \left(T_b - T_a\right)\frac{\ln\left(\frac{r}{a}\right)}{\ln\left(\frac{b}{a}\right)}. \tag{2}$$

To test the validity of plane stress and generalized plane strain assumptions, a 3D FEM analysis is carried out for different length to wall thickness ratios of cylinder.

3. Generalized-plane-strain analytical model considering strain hardening

Under the condition of generalized plane strain condition ($\varepsilon_z = \varepsilon_0 =$ constant), the thermo-elastic stresses in the cylinder are given by the equations provided in [23], when the cylinder is subjected to a sufficiently low temperature. At the inner radius the yielding of the material of the cylinder begins according to the Tresca criterion given by

$$\sigma_\theta - \sigma_r = k_1\sigma_{\text{eq}}, \quad \sigma_z - \sigma_r = k_1\sigma_{\text{eq}}, \tag{3}$$

where σ_{eq} is given by the Ludwik's hardening law (Eq. (1)). Beyond the inner radial position, the cylinder yields as per the Tresca yield criterion:

$$\sigma_z - \sigma_r = k_1\sigma_{\text{eq}}. \tag{4}$$

By substituting the thermo-elastic stresses in Eq. (3) at $r = a$, and taking $\sigma_{\text{eq}} = \sigma_Y$, the temperature difference required for the initiation of yielding at the inner radius can be obtained.

When the material of the cylinder yields as per the Tresca yield criterion, during first stage of elastic–plastic deformation the wall of the cylinder consists of three zones—plastic zone I ($a \le r \le c$), plastic zone II ($c \le r \le d$), and elastic zone ($d \le r \le b$). During the second stage of elasto-plastic deformation, the cylinder wall gets divided into five zones—two

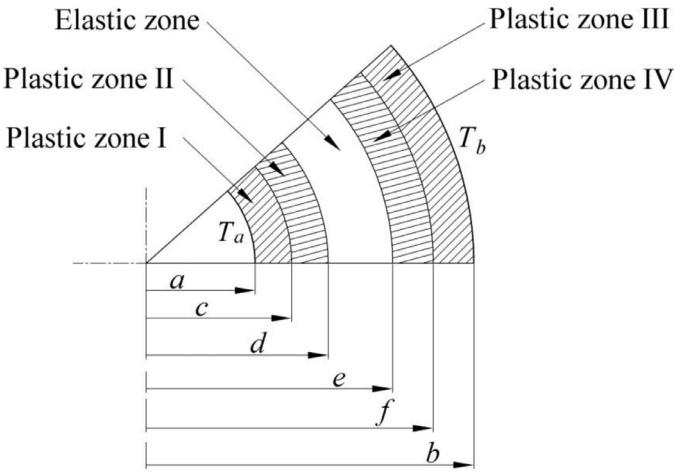

Fig. 1. Elastic and plastic zones in cylindrical segment during elastic–plastic deformation (generalized-plane-strain).

inner plastic zones: plastic zone I ($a \le r \le c$) and plastic zone II ($c \le r \le d$), an intermediate elastic zone: $d \le r \le e$ and two outer plastic zones: plastic zone III ($f \le r \le b$) and plastic zone IV ($e \le r \le f$). The two consecutive plastic zones in the cylinder correspond to two different sides of Tresca yield locus. The general geometry of the cylinder during elastic–plastic deformation is shown schematically in Fig. 1. In the following subsections the stresses and plastic strain fields in the first and second stage of elastic–plastic deformation are obtained by incorporating strain hardening using Ludwik's hardening law.

3.1. First stage of elastic–plastic deformation

The stresses and plastic strains in all the three zones during the first stage of elastic–plastic deformation are obtained in a similar manner as described in Kamal and Dixit [19]. The stresses in the elastic zone, $d \le r \le b$ are provided in [19]. However, the stresses and strains in the plastic zone get modified due to the incorporation of strain-hardening following the Ludwik's hardening law. The resulting fields of stresses and strains in the plastic zones I, $a \le r \le c$ and II, $c \le r \le d$ are obtained as follows:

Plastic zone I, $a \le r \le c$:

Using Eq. (3) in the stress equilibrium equation [19], the radial, hoop and axial stresses in the plastic zone I are obtained as

$$\sigma_r = k_1\sigma_Y \ln r + k_1 K \int_a^r \frac{\left(\varepsilon_{\text{eq}}^p\right)^n}{r_1}\mathrm{d}r_1 + C_3, \tag{5}$$

$$\sigma_\theta = \sigma_z = k_1\sigma_Y(1+\ln r) + k_1 K\left(\varepsilon_{\text{eq}}^p\right)^n + k_1 K\int_a^r \frac{\left(\varepsilon_{\text{eq}}^p\right)^n}{r_1}\mathrm{d}r_1 + C_3. \tag{6}$$

Using the condition of plastic incompressibility, the strain-displacement relation and the generalized Hooke's law, the expression for the radial displacement, the total hoop and radial strains can be obtained [19]. The plastic parts of the hoop, radial and axial strains are obtained by subtracting the elastic parts from the total strain components. They are given by

$$\begin{aligned}\varepsilon_\theta^p = {} & \frac{1-2\nu}{E}\left[\frac{1}{2}\left(k_1\sigma_Y\ln r + C_3\right) + \frac{2k_1K}{r^2}\int_a^r r_1\left(\varepsilon_{\text{eq}}^p\right)^n\mathrm{d}r_1\right.\\ & \left. -k_1K\int_a^r\frac{\left(\varepsilon_{\text{eq}}^p\right)^n}{r_1}\mathrm{d}r_1 + \frac{3k_1K}{r^2}\int_a^r\left\{r_2\int_a^{r_2}\frac{\left(\varepsilon_{\text{eq}}^p\right)^n}{r_1}\mathrm{d}r_1\right\}\mathrm{d}r_2\right]\\ & -\frac{3-2\nu}{4E}k_1\sigma_Y - \frac{1-\nu}{E}k_1K\left(\varepsilon_{\text{eq}}^p\right)^n + \frac{1}{2}\alpha T_a\\ & +\frac{\alpha\left(T_b-T_a\right)}{2\ln\left(\frac{b}{a}\right)}\left\{\ln\left(\frac{r}{a}\right)-\frac{3}{2}\right\} - \frac{1}{2}\varepsilon_0 + \frac{C_4}{r^2}.\end{aligned} \tag{7}$$

$$\begin{aligned}\varepsilon_r^p = {} & \frac{1-2\nu}{E}\left[\frac{1}{2}\left(k_1\sigma_Y\ln r + C_3\right) + 2k_1K\int_a^r\frac{\left(\varepsilon_{\text{eq}}^p\right)^n}{r_1}\mathrm{d}r_1\right.\\ & \left. -\frac{2k_1K}{r^2}\int_a^r r_1\left(\varepsilon_{\text{eq}}^p\right)^n\mathrm{d}r_1 - \frac{3k_1K}{r^2}\int_a^r\left\{r_2\int_a^{r_2}\frac{\left(\varepsilon_{\text{eq}}^p\right)^n}{r_1}\mathrm{d}r_1\right\}\mathrm{d}r_2\right]\\ & +\frac{7-6\nu}{4E}k_1\sigma_Y + \frac{2(1-\nu)}{E}k_1K\left(\varepsilon_{\text{eq}}^p\right)^n + \frac{1}{2}\alpha T_a\\ & +\frac{\alpha\left(T_b-T_a\right)}{2\ln\left(\frac{b}{a}\right)}\left\{\ln\left(\frac{r}{a}\right)+\frac{3}{2}\right\} - \frac{1}{2}\varepsilon_0 - \frac{C_4}{r^2}.\end{aligned} \tag{8}$$

$$\begin{aligned}\varepsilon_z^p = {} & \varepsilon_0 - \frac{1-2\nu}{E}\left\{k_1\sigma_Y\ln r + C_3 + k_1K\int_a^r\frac{\left(\varepsilon_{\text{eq}}^p\right)^n}{r_1}\mathrm{d}r_1\right\}\\ & -\frac{1-\nu}{E}k_1\sigma_Y - \frac{1-\nu}{E}k_1K\left(\varepsilon_{\text{eq}}^p\right)^n\\ & -\alpha T_a - \alpha\left(T_b-T_a\right)\frac{\ln\left(\frac{r}{a}\right)}{\ln\left(\frac{b}{a}\right)}.\end{aligned} \tag{9}$$

The equivalent plastic strain $\varepsilon_{\text{eq}}^p$ is given by

$$\varepsilon_{\text{eq}}^p = \sqrt{\frac{2}{3}\varepsilon_{ij}^p\varepsilon_{ij}^p}, \tag{10}$$

where ε_{ij}^p denotes the component of the plastic part of the strain tensor.

Plastic zone II, $c \le r \le d$:

Using the Tresca yield criterion (Eq. (4)) and its associated flow rule along with the strain compatibility [19], the elastic–plastic radial and hoop stresses are obtained as

$$\begin{aligned}\sigma_r = {} & C_5 r^{-1+\sqrt{2(1-\nu)}} + C_6 r^{-1-\sqrt{2(1-\nu)}} + \frac{k_1\sigma_Y}{(2\nu-1)}\\ & +\frac{k_1Kr^{-1+\sqrt{2(1-\nu)}}\left\{1-\nu+\nu\sqrt{2(1-\nu)}\right\}}{2\sqrt{2(1-\nu)}}\int_c^r r_1^{-\sqrt{2(1-\nu)}}\left(\varepsilon_{\text{eq}}^p\right)^n\mathrm{d}r_1\\ & -\frac{k_1Kr^{-1-\sqrt{2(1-\nu)}}\left\{1-\nu-\nu\sqrt{2(1-\nu)}\right\}}{2\sqrt{2(1-\nu)}}\int_c^r r_1^{\sqrt{2(1-\nu)}}\left(\varepsilon_{\text{eq}}^p\right)^n\mathrm{d}r_1\\ & +\frac{E\alpha T_a}{(2\nu-1)} + \frac{E\alpha\left(T_b-T_a\right)}{(2\nu-1)}\frac{\ln\left(\frac{r}{a}\right)}{\ln\left(\frac{b}{a}\right)}\\ & -\frac{2E\alpha\left(T_b-T_a\right)}{(2\nu-1)^2\ln\left(\frac{b}{a}\right)} - \frac{E\alpha\left(T_b-T_a\right)}{(2\nu-1)\ln\left(\frac{b}{a}\right)} - \frac{E\varepsilon_0}{(2\nu-1)},\end{aligned} \tag{11}$$

$$\begin{aligned}\sigma_\theta = {} & C_5\sqrt{2(1-\nu)}r^{\sqrt{2(1-\nu)}-1} - C_6\sqrt{2(1-\nu)}r^{-\sqrt{2(1-\nu)}-1} + \frac{k_1\sigma_Y}{(2\nu-1)}\\ & +\frac{k_1K\sqrt{2(1-\nu)}r^{\sqrt{2(1-\nu)}-1}\left\{1-\nu+\nu\sqrt{2(1-\nu)}\right\}}{2\sqrt{2(1-\nu)}}\\ & \times\int_c^r r_1^{-\sqrt{2(1-\nu)}}\left(\varepsilon_{\text{eq}}^p\right)^n\mathrm{d}r_1\\ & +\frac{k_1K\sqrt{2(1-\nu)}r^{-\sqrt{2(1-\nu)}-1}\left\{1-\nu-\nu\sqrt{2(1-\nu)}\right\}}{2\sqrt{2(1-\nu)}}\\ & \times\int_c^r r_1^{\sqrt{2(1-\nu)}}\left(\varepsilon_{\text{eq}}^p\right)^n\mathrm{d}r_1 + \nu k_1K\left(\varepsilon_{\text{eq}}^p\right)^n\\ & +\frac{E\alpha T_a}{(2\nu-1)} + \frac{E\alpha\left(T_b-T_a\right)}{(2\nu-1)}\frac{\ln\left(\frac{r}{a}\right)}{\ln\left(\frac{b}{a}\right)} - \frac{2E\alpha\left(T_b-T_a\right)}{(2\nu-1)^2\ln\left(\frac{b}{a}\right)} - \frac{E\varepsilon_0}{(2\nu-1)}.\end{aligned} \tag{12}$$

The expression for σ_z can be obtained from the Tresca criterion given by Eq. (4).

Using the Tresca associated flow rule, the plastic part of the hoop strain in the plastic zone is obtained as zero implying $\varepsilon_r^p = -\varepsilon_z^p$. In this zone, the plastic strains are given by

$$\begin{aligned}\varepsilon_r^p = -\varepsilon_z^p = {} & \frac{C_5}{E} r^{-1+\sqrt{2(1-\nu)}} \left\{1-\nu-\nu\sqrt{2(1-\nu)}\right\} \\ & + \frac{C_6}{E} r^{-1-\sqrt{2(1-\nu)}} \left\{1-\nu+\nu\sqrt{2(1-\nu)}\right\} \\ & + \frac{k_1 K r^{-1+\sqrt{2(1-\nu)}} \left\{1-\nu-\nu\sqrt{2(1-\nu)}\right\}\left\{1-\nu+\nu\sqrt{2(1-\nu)}\right\}}{2\sqrt{2(1-\nu)}E} \\ & \times \int_c^r r_1^{-\sqrt{2(1-\nu)}} \left(\varepsilon_{\text{eq}}^p\right)^n \mathrm{d}r_1 \\ & - \frac{k_1 K r^{-1-\sqrt{2(1-\nu)}} \left\{1-\nu+\nu\sqrt{2(1-\nu)}\right\}\left\{1-\nu-\nu\sqrt{2(1-\nu)}\right\}}{2\sqrt{2(1-\nu)}E} \\ & \times \int_c^r r_1^{\sqrt{2(1-\nu)}} \left(\varepsilon_{\text{eq}}^p\right)^n \mathrm{d}r_1 \\ & + \left(1-\nu^2\right)\frac{k_1 K}{E}\left(\varepsilon_{\text{eq}}^p\right)^n + \frac{\alpha\left(T_b - T_a\right)}{\ln\left(\frac{b}{a}\right)} \frac{(1+\nu)}{(2\nu-1)}, \end{aligned} \tag{13}$$

The constants C_5 and C_6 are determined by using the continuity of radial stresses and plastic strains at the elastic–plastic interface. The continuity of radial stresses at the interface of the plastic zones I and II provides the constant C_3 and the continuity of plastic hoop strain provides the constant C_4. The constant axial strain ε_0 is obtained by using the free-end condition, i.e., making the resultant of the axial stresses zero.

To evaluate the unknown boundary radii, c and d, a numerical procedure needs to be used. The procedure involves an iterative approach to estimate the values of c and d. The initial estimates for c and d can be obtained from non-hardening case ($K=0$) by using the boundary conditions of vanishing radial stress at the inner radius and $\sigma_\theta^{(\text{plastic zone II})} = \sigma_z^{(\text{plastic zone II})}$ at $r=c$ and solving them using FSOLVE function in MATLAB®. The initial guess value of $\varepsilon_{\text{eq}}^p$ is taken as zero everywhere in the plastic zones I and II. With these values of c and d, the values of ε_θ^p, ε_r^p and ε_0^p are updated in Eqs. (7)–(9) for plastic zone I. Eq. (10) provides the updated values of $\varepsilon_{\text{eq}}^p$ at any radial position in the plastic zone I. Similarly, using Eq. (13), the values of ε_r^p at different radial positions in the plastic zone II are updated. The updated values of $\varepsilon_{\text{eq}}^p$ at different radial positions in the plastic zone II are obtained from Eq. (10). These values of equivalent plastic strain are used to obtain the updated components of plastic strain. From these components, the values of $\varepsilon_{\text{eq}}^p$ are updated further for fixed c and d in both the plastic zones. This procedure is repeated till the convergence in $\varepsilon_{\text{eq}}^p$ is achieved. The integral terms involved in the expressions can be evaluated numerically by using two-Gauss-point formula. Now, using the converged values of $\varepsilon_{\text{eq}}^p$, the boundary conditions of vanishing radial stress at the inner radius and $\sigma_\theta^{(\text{plastic zone II})} = \sigma_z^{(\text{plastic zone II})}$ at $r=c$ are solved again to get the new estimates of c and d. If these new estimates of c and d are same as the previously estimated values of c and d the procedure is stopped, otherwise the whole procedure is repeated till the convergence for c and d is achieved.

3.2. Second stage of elastic–plastic deformation

In the second stage of elastic–plastic deformation, the outer plastic zone, i.e., plastic zone III ($f \le r \le b$), develops in the wall of the cylinder according to the Tresca yield criterion given by

$$\sigma_\theta - \sigma_r = -k_1\sigma_{\text{eq}}, \quad \sigma_z - \sigma_r = -k_1\sigma_{\text{eq}} \tag{14}$$

Another plastic zone, i.e., plastic zone IV ($e \le r \le f$) develops simultaneously along with the plastic zone III as per the Tresca yield criterion:

$$\sigma_\theta - \sigma_r = -k_1\sigma_{\text{eq}}. \tag{15}$$

The stress and strain expressions for the plastic zones I and II during the second stage of elastic–plastic deformation are same as in the case of first stage of elastic–plastic deformation. However, the constants C_3, C_4, C_5 and C_6 change due to change of continuity conditions. The stress solutions in the intermediate elastic zone are available in Ref. [19]. The equations for stresses and plastic strains incorporating the Ludwik's hardening law in the plastic zones III and IV are obtained as follows:

Plastic zone III, $f \le r \le b$:

Using the Tresca yield criterion (Eq. (14)) and the stress equilibrium equation, the radial, hoop and axial stresses are given by

$$\sigma_r = -k_1\sigma_Y \ln r - k_1 K \int_f^r \frac{\left(\varepsilon_{\text{eq}}^p\right)^n}{r_1}\mathrm{d}r_1 + C_7, \tag{16}$$

$$\sigma_\theta = \sigma_z = -k_1\sigma_Y(1+\ln r) - k_1 K\left(\varepsilon_{\text{eq}}^p\right)^n - k_1 K \int_f^r \frac{\left(\varepsilon_{\text{eq}}^p\right)^n}{r_1}\mathrm{d}r_1 + C_7. \tag{17}$$

The plastic parts of the hoop, radial and axial strains are obtained in a similar way as described in Section 3.1 and are given by

$$\begin{aligned}\varepsilon_\theta^p = {} & \frac{1-2\nu}{E}\left[\frac{1}{2}\left(C_7 - k_1\sigma_Y \ln r\right) - \frac{2k_1 K}{r^2}\int_f^r r_1\left(\varepsilon_{\text{eq}}^p\right)^n \mathrm{d}r_1\right. \\ & + k_1 K \int_f^r \frac{\left(\varepsilon_{\text{eq}}^p\right)^n}{r_1}\mathrm{d}r_1 - \frac{3k_1 K}{r^2}\int_f^r \left\{r_2 \int_f^{r_2} \frac{\left(\varepsilon_{\text{eq}}^p\right)^n}{r_1}\mathrm{d}r_1\right\}\mathrm{d}r_2\Bigg] \\ & + \frac{3-2\nu}{4E}k_1\sigma_Y + \frac{1-\nu}{E}k_1 K\left(\varepsilon_{\text{eq}}^p\right)^n + \frac{1}{2}\alpha T_a \\ & + \frac{\alpha\left(T_b - T_a\right)}{2\ln\left(\frac{b}{a}\right)}\left\{\ln\left(\frac{r}{a}\right) - \frac{3}{2}\right\} - \frac{1}{2}\varepsilon_0 + \frac{C_8}{r^2}, \end{aligned} \tag{18}$$

$$\begin{aligned}\varepsilon_r^p = {} & \frac{1-2\nu}{E}\left[\frac{1}{2}\left(C_7 - k_1\sigma_Y \ln r\right) - 2k_1 K \int_f^r \frac{\left(\varepsilon_{\text{eq}}^p\right)^n}{r_1}\mathrm{d}r_1\right. \\ & + \frac{2k_1 K}{r^2}\int_f^r r_1\left(\varepsilon_{\text{eq}}^p\right)^n \mathrm{d}r_1 + \frac{3k_1 K}{r^2}\int_f^r \left\{r_2 \int_f^{r_2} \frac{\left(\varepsilon_{\text{eq}}^p\right)^n}{r_1}\mathrm{d}r_1\right\}\mathrm{d}r_2\Bigg] \\ & - \frac{7-6\nu}{4E}k_1\sigma_Y - \frac{2(1-\nu)}{E}k_1 K\left(\varepsilon_{\text{eq}}^p\right)^n + \frac{1}{2}\alpha T_a \\ & + \frac{\alpha\left(T_b - T_a\right)}{2\ln\left(\frac{b}{a}\right)}\left\{\ln\left(\frac{r}{a}\right) + \frac{3}{2}\right\} - \frac{1}{2}\varepsilon_0 - \frac{C_8}{r^2}, \end{aligned} \tag{19}$$

$$\begin{aligned}\varepsilon_z^p = {} & \varepsilon_0 - \frac{1-2\nu}{E}\left\{-k_1\sigma_Y \ln r + C_7 - k_1 K \int_f^r \frac{\left(\varepsilon_{\text{eq}}^p\right)^n}{r_1}\mathrm{d}r_1\right\} + \frac{1-\nu}{E}k_1\sigma_Y \\ & + \frac{1-\nu}{E}k_1 K\left(\varepsilon_{\text{eq}}^p\right)^n - \alpha T_a - \alpha\left(T_b - T_a\right)\frac{\ln\left(\frac{r}{a}\right)}{\ln\left(\frac{b}{a}\right)}. \end{aligned} \tag{20}$$

Plastic zone IV, $e \le r \le f$:

Using Eq. (15) in stress equilibrium equation, the radial stress is given by

$$\begin{aligned}\sigma_r = {} & \frac{E\alpha}{(2\nu-1)}T_a + \frac{E\alpha\left(T_b - T_a\right)}{2(1-\nu)\ln\left(\frac{b}{a}\right)}\left[\frac{1}{(2\nu-1)}\left\{\ln\left(\frac{d}{a}\right) + \frac{1}{2} - \frac{e^2}{2d^2}\right\} - \ln\left(\frac{e}{a}\right)\right] \\ & + \left\{\frac{1}{2\nu-1}\left(1 + \frac{e^2}{2d^2}\right) + \frac{1}{2} - \ln\left(\frac{r}{e}\right)\right\}k_1\sigma_Y + \frac{E\varepsilon_0}{(1-2\nu)} - k_1 K\int_e^r \frac{\left(\varepsilon_{\text{eq}}^p\right)^n}{r_1}\mathrm{d}r_1. \end{aligned} \tag{21}$$

Knowing the expression for σ_r, the expression for σ_θ can be obtained from Eq. (15). The Tresca associated flow rule indicates that the axial strain in the plastic zone IV is wholly elastic. Hence, the axial stress

Table 1
Material properties of aluminum.

Yield stress, σ_Y (MPa)	Modulus of elasticity, E (GPa)	Poisson's ratio, ν	Coefficient of thermal expansion, α (/°C)	Mass density, ρ (kg/m^3)	Thermal conductivity, k (W/m. K)	Specific heat, c_p (J/kg. K)
50.3	69	0.30	22.2×10^{-6}	2700	205	900

component can be obtained by using the generalized Hooke's law [19]. The resulting expression for axial stress is given by

$$\sigma_z = \frac{E\alpha}{(2\nu-1)}T_a + \frac{E\alpha(T_b-T_a)}{2(1-\nu)\ln\left(\frac{b}{a}\right)}\left[\frac{2\nu}{(2\nu-1)}\left\{\ln\left(\frac{d}{a}\right)+\frac{1}{2}-\frac{e^2}{2d^2}\right\} +2\nu\ln\left(\frac{r}{e}\right)-2\ln\left(\frac{r}{a}\right)\right] +\left\{\frac{2\nu}{2\nu-1}\left(1+\frac{e^2}{2d^2}\right)-2\nu\ln\left(\frac{r}{e}\right)\right\}k_1\sigma_Y+\frac{E\varepsilon_0}{(1-2\nu)} -2\nu k_1K\int_e^r\frac{\left(\varepsilon_{eq}^p\right)^n}{r_1}dr_1-\nu k_1K\left(\varepsilon_{\text{eq}}^p\right)^n. \quad (22)$$

The plastic part of the hoop strain, $\varepsilon_\theta^p(=-\varepsilon_r^p)$ is given by

$$\varepsilon_\theta^p = \frac{\alpha(T_b-T_a)}{2(1-\nu)\ln\left(\frac{b}{a}\right)}(\nu^2-1)+(1-\nu^2)\frac{k_1\sigma_Y}{E} +\frac{4\nu^2}{Er^2}k_1K\int_e^r\left\{r_2\int_e^{r_2}\frac{\left(\varepsilon_{\text{eq}}^p\right)^n}{r_1}dr_1\right\}dr_2 +\frac{2\nu^2}{Er^2}k_1K\int_e^r r_1\left(\varepsilon_{\text{eq}}^p\right)^n dr_1+(1-\nu^2)\frac{k_1K}{E}\left(\varepsilon_{\text{eq}}^p\right)^n -\frac{2\nu^2k_1K}{E}\int_e^r\frac{\left(\varepsilon_{\text{eq}}^p\right)^n}{r_1}dr_1+\frac{C_9}{r^2}. \quad (23)$$

The constants C_5 and C_6 are obtained by employing the continuity condition of radial stresses and radial plastic strains at the elastic–plastic interface radius d. The constant C_3 is obtained by using continuity of radial stresses at $r=c$. The continuity condition of the plastic hoop strains at $r=c$ provides the constant C_4. To obtain the constant C_7, continuity of the radial stresses at $r=f$ can be employed. The constants C_9 and C_8 can be obtained by using the boundary conditions of continuity of the plastic part of the hoop strains at the interface radii e and f, respectively. The constant axial strain ε_0 in the second stage of elastic–plastic deformation can be obtained by using the free-end condition. The interface radii c, d, e and f are obtained in a manner similar to that described in Section 3.1.

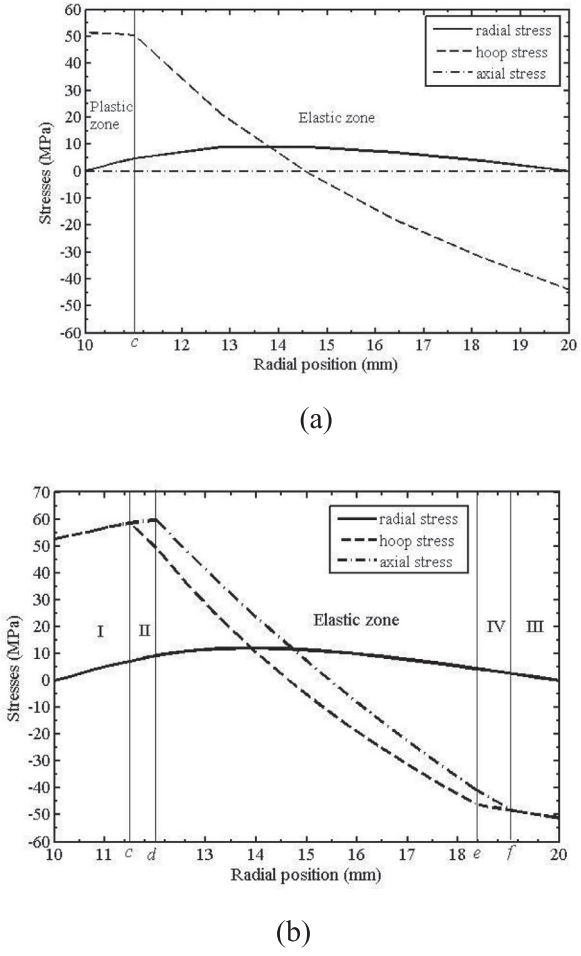

Fig. 2. Elastic–plastic stresses in aluminum cylinder: (a) plane-stress, (b) generalized-plane-strain.

4. Numerical simulations

In this section, numerical simulations with the plane-stress and generalized-plane-strain models are carried out for a typical cylinder. The objective is to compare the solutions for stresses and plastic strains of these two models under a radial thermal gradient. An aluminum cylinder with $a=10$ mm and $b=20$ mm is considered. The material properties of aluminum are provided in Table 1.

The hardening coefficient K and strain hardening exponent n for the cylinder are taken as 58.18 MPa and 0.482 [18]. The temperature difference required to initiate the yielding at the inner wall of the cylinder is obtained as 53.66 °C for plane stress model and 37.56 °C for generalized plane strain model. The simulation is carried out for a temperature difference, $(T_b-T_a)=75$ °C. With this temperature gradient mechanical and thermal properties do not vary much [24]. The inner wall is assumed to be at $T_a=25$ °C. According to plane stress model, for $(T_b-T_a)=75$ °C, the cylinder undergoes first stage of elastic–plastic deformation with an inner plastic zone propagating outwards up to a radius $c=11.0121$ mm. However, as per generalized plane strain model, the cylinder undergoes second stage of elastic–plastic deformation dividing the cylinder wall into two inner-plastic, two outer-plastic and an intermediate-elastic zone. At the inner wall, plastic zone I propagates outwards to a radius $c=11.4973$ mm and plastic zone II propagates outwards to a radius $d=12.0215$ mm. A plastic zone III propagates inwards from the outer radius to a radius $f=19.0966$ mm and plastic zone IV propagates inwards to a radius $e=18.3296$ mm.

The elastic–plastic stresses generated in different zones of the cylinder for plane stress and generalized plane strain conditions are shown along a radial path in Fig. 2. It is observed from Fig. 2(a) that for plane stress case, the maximum value of hoop stress in the cylinder is generated at the inner radius of the cylinder and is tensile in nature. Fig. 2(b) shows that the maximum value of hoop stress exists at the interface radius c and the maximum value of axial stress exists at the interface radius d as per generalized plane strain model. The magnitudes of radial stresses along the radial path are smaller for plane stress as well as generalized plane strain model.

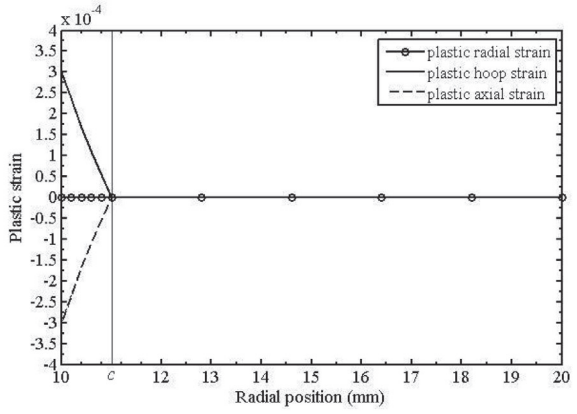

(a)

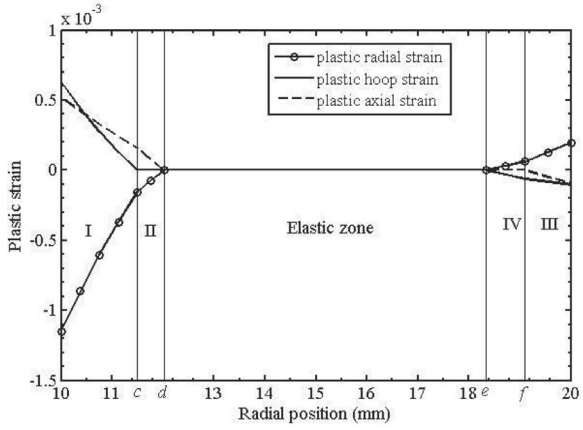

(b)

Fig. 3. Plastic strain distribution in aluminum cylinder: (a) plane-stress, (b) generalized-plane-strain.

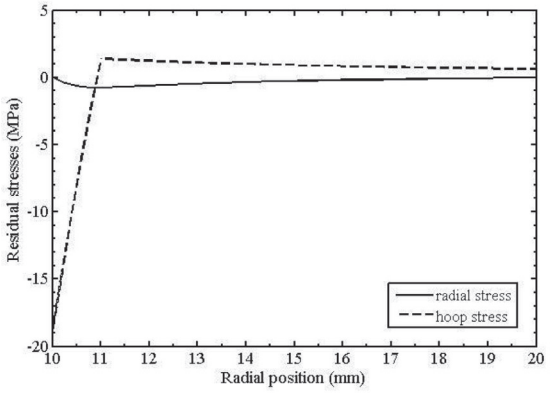

(a)

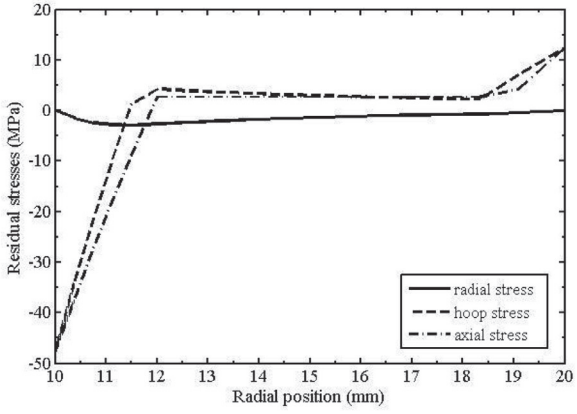

(b)

Fig. 4. Residual stress distribution in aluminum cylinder: (a) plane-stress, (b) generalized-plane-strain.

The plastic parts of radial, hoop and axial strains produced in the cylinder are obtained for both plane stress and generalized plane strain models (Fig. 3). It is observed from Fig. 3(a) that the plastic parts of strains are numerically very small for plane stress case. However, Fig. 3(b) shows that for generalized plane strain case, although the plastic parts of strains are larger in magnitude as compared to plane stress case, their magnitudes are still small (of the order of 10^{-3}). Thus, the magnitude of equivalent plastic strain generated in the cylinder is also not very substantial. As the value of equivalent stress σ_{eq} in the plastic zone for yielding depends on the equivalent plastic strain, here the value of σ_{eq} will not deviate much from σ_Y. The maximum deviation of σ_{eq} from σ_Y is only 2% for the plane stress condition and 4.87% for the generalized plane strain condition. The maximum equivalent plastic strain occurs at the inner radius.

When the temperature difference $(T_b - T_a)$ is removed, i.e., when the cylinder is cooled to room temperature, the residual stresses are set up in the wall of the cylinder. Considering the unloading process to be completely elastic, the residual stresses can be obtained by subtracting the thermo-elastic stresses [21] from the respective stress equations of elastic–plastic zones. The resulting residual stress distribution in the cylinder for the plane stress and the generalized plane strain condition is shown in Fig. 4. It is observed from Fig. 4(a) and (b) that the compressive residual hoop stresses are generated at and around the inner radius of the cylinder. For the same temperature difference, the generalized plane strain model predicts larger magnitude of compressive residual hoop stress at the inner radius. Fig. 4(b) shows that for generalized plane strain condition the axial residual stresses generated at and around the inner radius of the cylinder are also compressive. The compressive residual stresses at and around the inner radius of the cylinder helps in reducing the net maximum stress produced in the cylinder in the next loading stage. This amounts to increase the load carrying capacity of the cylinder. The magnitudes of tensile hoop and axial stresses are small at and around the outer wall of the cylinder.

5. Three-dimensional finite-element modeling of elastic plastic stresses in thick cylinders due to temperature gradient

From the numerical simulations of both the plane stress and generalized plane strain analytical models, it is not clear which model is valid for a particular length of the cylinder. To assess the validity of the analytical models, a 3D FEM analysis using ABAQUS 6.10 package is carried out. A homogeneous thick-walled hollow cylinder with inner radius a and outer radius b is considered. The inner wall is subjected to a temperature T_a and the outer wall is subjected to a temperature T_b such that $T_b > T_a$. The problem is solved using ABAQUS standard code. Under the radial temperature difference, $(T_b - T_a)$, the steady state condition is assumed in ABAQUS standard simulation. The strain hardening of the material during plastic deformation is considered. For comparison of the FEM results with the plane-stress and generalized-plane-strain models, the analytical solution developed in [18] and the stress solution devel-

Table 2
Mesh sensitivity analysis.

Mesh	Number of elements in			Maximum value of			Screentime (s)
	Radial direction	Circumferential direction	Axial direction	Radial stress (MPa)	Hoop stress (MPa)	Axial stress (MPa)	
Mesh 1	6	4	25	20.61	48.71	58.20	2
Mesh 2	12	4	25	11.45	59.50	58.04	5
Mesh 3	24	4	25	10.48	62.40	58.00	16
Mesh 4	48	4	25	10.58	63.14	57.99	34
Mesh 5	24	8	25	12.39	59.71	58.34	35
Mesh 6	24	16	25	12.63	61.07	59.18	247
Mesh 7	24	32	25	12.74	62.24	61.28	926
Mesh 8	24	64	25	12.90	62.90	62.29	2959
Mesh 9	**24**	**32**	**50**	**12.74**	**62.76**	**61.21**	**3664**
Mesh 10	24	32	100	12.73	62.93	61.19	4346

Mesh 9 indicated in the boldfaced is the optimum mesh.

Table 3
Comparison of stresses between 3D FEM and analytical models.

$L/(b-a)$	L_2 norm of error in stresses between FEM and plane stress (MPa)			L_2 norm of error in stresses between FEM and generalized plane strain (MPa)		
	σ_r	σ_θ	σ_z	σ_r	σ_θ	σ_z
10	5.5849	26.7094	134.5956	**2.4418**	**4.3992**	**2.5369**
8	5.5148	27.3775	136.0487	**2.5578**	**4.7597**	**2.7440**
6	5.9687	29.4939	137.3141	**2.4754**	**7.6960**	**4.1740**
5	7.4358	28.3009	133.9557	4.9296	8.7777	11.7016
4	7.8224	40.6167	112.6305	3.8787	31.2258	24.3158
2	4.6443	36.8936	30.4968	4.9293	43.5744	110.0771
1	**3.4278**	**5.1446**	**3.6140**	8.2861	33.3531	135.7536
0.5	**2.7080**	**3.7979**	**1.3881**	7.1190	33.2992	136.0458

The boldfaced values correspond to the cases in which all stress components show less than 10% error.

oped in Section 3 are used. The detailed analysis of 3D FEM is presented in the following subsections.

5.1. 3D finite-element modeling

A 3D FEM model for analysing thermo-elastic–plastic stresses in the cylinder under the radial temperature difference was developed using commercial finite element package ABAQUS 6.10. A coupled thermo-mechanical approach is used to obtain the steady-state thermal stress solutions in ABAQUS/Standard. In thermal autofrettage process, the cylinder is subjected to non-homogeneous elastic–plastic deformation due to radial thermal gradient between the outer and inner wall of the cylinder. Hence, for the stress solution in thermal autofrettage process, coupled temperature-displacement elements of ABAQUS/Standard [25] are used. The part considered for the 3D FEM analysis is a thick-walled solid extruded cylinder with open ends.

5.2. Material properties

An aluminum cylinder is considered. The inner and outer radii of the cylinder are taken as 10 mm and 20 mm, respectively. The temperature difference across the wall thickness of the cylinder is taken as 75 °C. The thermal stress analysis during the thermal loading and unloading of cylinder for different lengths is carried out. The mechanical and thermal properties of aluminum are presented in Table 1. The model used von Mises criterion with isotropic hardening.

5.3. Boundary conditions and mesh generation

The thermal stresses in the cylinder are induced due to the radial thermal gradient across the wall thickness. For analyzing the thermal stress, the Dirichlet temperature boundary conditions are specified at the inner and outer surfaces of the cylinder. The temperature of the inner surface is prescribed as $T_a = 25$ °C and that of the outer surface is prescribed as $T_b = 100$ °C. At each node, there are three translational degrees of freedom, viz., radial displacement u_r, circumferential displacement u_θ and axial displacement u_z. In the analysis, the circumferential displacement, u_θ vanishes. This implies that the rotation in the circumferential direction is constrained, but the cylinder is free to expand axially and radially. A schematic of the 3D part in ABAQUS along with the thermal and displacement boundary conditions is shown in Fig. 5.

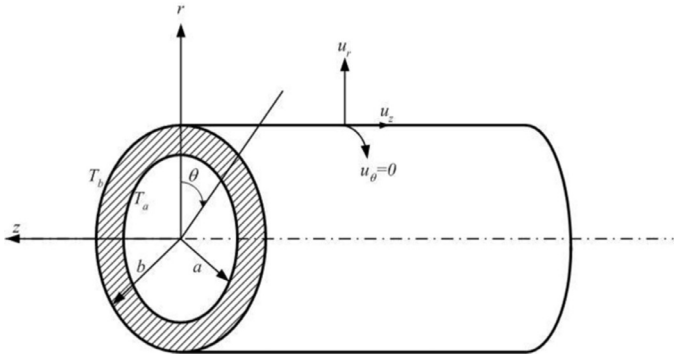

Fig. 5. Schematic of 3D part in ABAQUS along with the boundary conditions.

An eight-node continuum C3D8T thermally coupled brick, trilinear displacement and temperature element is used to generate the mesh on the cylinder. The meshed cylinder is shown in Fig. 6. Although the cylinder is modeled as open-ended, the axial stresses are produced in it due to the thermal gradient. When the inner surface of the cylinder is at a temperature lower than that of the outer surface, the tendency to expand in the axial direction is less in the vicinity of the inner surface than in the vicinity of the outer one. This causes tensile axial stresses on the inner side and compressive axial stresses at the outer side. However, the resultant axial force due to these stresses is zero.

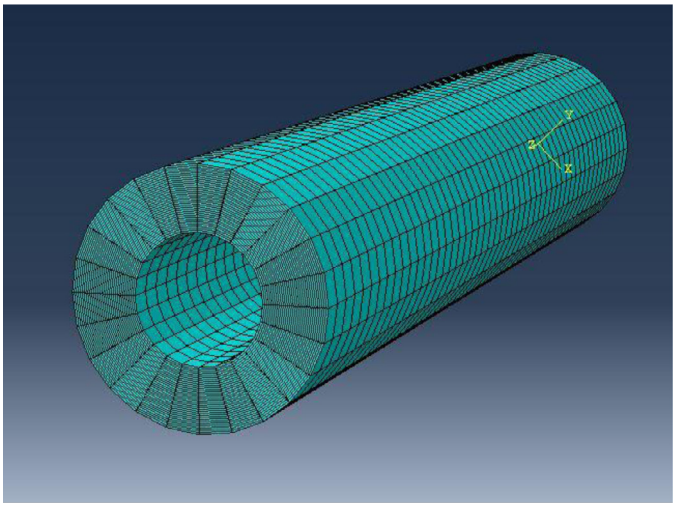

Fig. 6. Cylindrical geometry with typical C3D8T element.

5.4. Mesh sensitivity analysis

A mesh sensitivity analysis is carried out in order to select an appropriate mesh size. The mesh sensitivity analysis is presented in Table 2 based on the maximum values of radial, hoop and axial stresses generated in the cylinder. The length of the cylinder was taken as 100 mm. It is observed from Table 2 that the Mesh 9 with 24 elements in the radial direction, 32 elements in the circumferential direction and 50 elements in the axial direction leads to the convergent mesh. This mesh has a total of 38,400 elements. Mesh 9 provides less than 1% deviation in the solution in comparison to Mesh 8 and Mesh 10. Hence, it is considered as the optimum mesh. The thermo-elastic–plastic stresses generated in the cylinder are analyzed varying the length of the cylinder using Mesh 9. A comparative study with the plane stress and generalized plain strain models is presented for different length to wall-thickness ratios of the cylinder in Section 5.5.

5.5. Comparison of 3D finite element elastic–plastic thermal stresses with plane-stress and generalized-plane-strain models for different length to wall thickness ratios of cylinder

The 3D FEM simulations are carried out for different length to wall thickness ratios of the cylinder and the results are compared with analytical plane stress and generalized plane strain model. The present FEM analysis is carried out in 2.40-GHz processor and 2.60-GB random-access memory (RAM) ACER PC and it takes about 1 h of screen time. However, the analytical models provide the solution in less than 10 min. The comparison of radial, hoop and axial stresses between 3D FEM and analytical models along the radial path for different length to wall thickness ratio is shown in Table 3 using L_2 norm of error in stresses. The stresses along a radial path from the 3D ABAQUS finite element model are obtained considering a radial path at the mid-length of the cylinder. The stresses along a radial path at the edges become sufficiently low in FEM model and are not taken into account for the analysis.

It is observed from Table 3 that L_2 norm of error in stresses between 3D FEM and generalized plane strain are reasonably small when the length to wall thickness ratio of the cylinder is greater than or equal to 6. Thus, the generalized plane strain model is well established for $L/(b-a) \geq 6$. It is also observed from Table 3 that when $L/(b-a) \leq 1$, the L_2 norm of error between 3D FEM and plane stress becomes smaller. This shows that the plane stress analytical model is valid for length to wall thickness ratio, $L/(b-a) \leq 1$. The comparison of 3D finite element solutions with the generalized plane strain model for $L/(b-a) = 10$ is shown in Fig. 7(a). Fig. 7(b) shows the comparison of 3D finite element

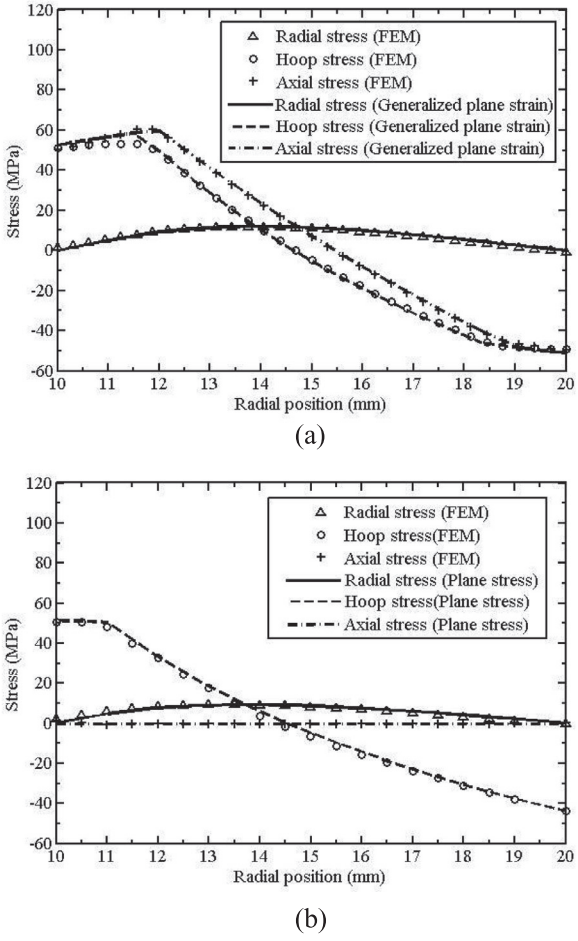

Fig. 7. Comparison of elastic–plastic stresses between 3D FEM and (a) generalized-plane-strain for $L/(b-a) = 10$, (b) plane-stress for $L/(b-a) = 0.5$ in aluminum cylinder.

results with the plane stress model for $L/(b-a) = 0.5$ in aluminum cylinder.

5.6. Residual stress solutions

The whole cylinder is cooled to room temperature (25 °C) by imposing the cooling boundary condition in ABAQUS/Standard. This generates the residual stresses in the cylinder. The finite element residual stresses in the cylinder are obtained along a radial path at the mid-length. The results for long and short cylinders are depicted in Fig. 8 along with the predictions of generalized plane strain model for $L/(b-a) = 10$ and plane stress model for $L/(b-a) = 0.5$. It is observed that the finite element predictions of the residual stresses are in close agreement with the analytical models.

6. Conclusions

The main objective of this work is to compare thermo-elastic–plastic plane-stress and generalized-plane-strain analyses with 3D FEM simulations. For the plane-stress analysis, the model of Kamal and Dixit [18] is used. For the generalized-plane-strain analysis, the model of Kamal and Dixit [19] is extended to incorporate the effect of strain hardening. The FEM results are compared with the analytical solutions for different length to wall thickness ratio, $L/(b-a)$, of the cylinder. The comparison suggests the applicability of the developed analytical models on the basis of $L/(b-a)$ ratio of the cylinder. The generalized plane strain analytical model provides realistic solution for $L/(b-a) \geq 6$. Thus, this

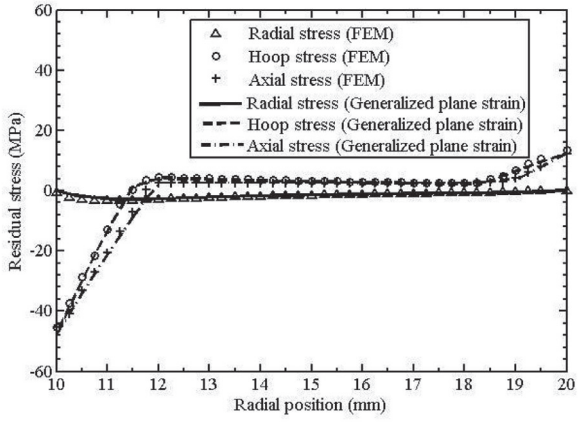

(a)

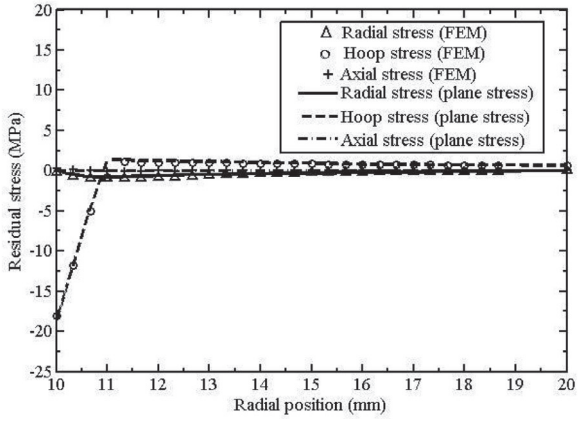

(b)

Fig. 8. Comparison of residual stresses between 3D FEM and (a) generalized-plane-strain for $L/(b-a)=10$, (b) plane-stress for $L/(b-a)=0.5$ in aluminum cylinder.

model is suitable for long cylinders such as gun barrels, pressure vessels and thick pipes subjected to thermal gradient. The plane stress analytical model provides good results for very short cylinders (thin disks) such as fastener holes with $L/(b-a)\leq 1$. It is to be noted that the CPU time required is much more in case of FEM analysis compared to the solution obtained by analytical models. Thus, the analytical models have their own importance mainly due to computational efficiency. The validity of the plane-stress and the generalized-plane-strain assumptions is inferred based on the same material model and the fixed b/a ratio. This study highlights that for $L/(b-a)$ ratio between 1 and 6, a 3D analysis is required. For other types of cylinder, the range of $L/(b-a)$ requiring 3D analysis may differ. It will be interesting to carry out a similar study for a number of cylinder geometries, loading conditions and material model formulations, and develop a generalized criterion for the validity of each model.

Acknowledgments

Funding from the Engineering and Physical Sciences Research Council (UK) through grant EP/K028316/1 and Department of Science and Technology (India) through grant DST/RC-UK/14-AM/2012, project Modeling of Advanced Materials for Simulation of Transformative Manufacturing Processes (MAST) is gratefully acknowledged. The authors are also thankful to the organizers of WCCM XII & APCOM VI 2016 Congress for giving the opportunity of oral presentation of this paper.

References

[1] Hill R, Lee EH, Tupper SJ. The theory of combined plastic and elastic deformation with particular reference to a thick tube under internal pressure. Proc R Soc A 1947;191(November):278–303.
[2] Gao XL. An exact elasto-plastic solution for an open-ended thick-walled cylinder of a strain-hardening material. Int J Press Vessel Pip 1992;52:129–44.
[3] Durban D. Large strain solution for pressurized elasto/plastic tubes. J Appl Mech 1979;46:228–30.
[4] Gao XL. An exact elasto-plastic solution for a closed-end thick-walled cylinder of elastic linear-hardening material with large strains. Int J Press Vessel Pip 1993;56:331–50.
[5] Bonn R, Haupt P. Exact solutions for large elastoplastic deformations of a thick--walled tube under internal pressure. Int J Plast 1995;11:99–118.
[6] Gao XL. Elasto-plastic analysis of an internally pressurized thick-walled cylinder using a strain gradient plasticity theory. Int J Solids Struct 2003;40:6445–55.
[7] Darijani H, Kargarnovin MH, Naghdabadi R. Design of thick-walled cylinders under internal pressure based on elasto-plastic approach. Mater Des 2009;30:3537–44.
[8] Bland DR. Elastoplastic thick-walled tubes of work-hardening material subject to internal and external pressures and to temperature gradients. J Mech Phys Solids 1956;4:209–29.
[9] Wong H, Simionescu O. An analytical solution of thermoplastic thick-walled tube subject to internal heating and variable pressure, taking into account corner flow and nonzero initial stress. Int J Eng Sci 1996;34:1259–69.
[10] Orçan Y, Eraslan AN. Thermal stresses in elastic-plastic tubes with temperature-dependent mechanical and thermal properties. J Therm Stresses 2001;24:1097–113.
[11] Sadeghian M, Toussi HE. Elasto-plastic axisymmetric thermal stress analysis of functionally graded cylindrical vessel. J Basic Appl Sci Res 2012;2:10246–57.
[12] Anani Y, Rahimi GH. Stress analysis of thick pressure vessel composed of functionally graded incompressible hyperelastic materials. Int J Mech Sci 2015;104:1–7.
[13] Orçan Y. Thermal stresses in a heat generating elastic-plastic cylinder with free ends. Int J Eng Sci 1994;32:883–98.
[14] Cowper GR. The elastoplastic thick-walled sphere subjected to a radial temperature gradient. J Appl Mech 1960:496–500.
[15] Johnson W, Mellor PB. Elastic-plastic behaviour of thick-walled spheres of non–work-hardening material subject to a steady-state radial temperature gradient. Int J Mech Sci 1962;4:147–58.
[16] Darijani H, Kargarnovin MH, Naghdabadi R. Design of spherical vessels under steady-state thermal loading using thermo-elasto–plastic concept. Int J Press Vessel Pip 2009;86:143–52.
[17] Zare HR, Darijani H. Strengthening and design of the linear hardening thick--walled cylinders using the new method of rotational autofrettage. Int J Mech Sci 2017:124–125: 1–8.
[18] Kamal SM, Dixit US. Feasibility study of thermal autofrettage process. In: Narayanan RG, Dixit US, editors. Advances in material forming and joining. New Delhi: Springer; 2015. p. 81–107.
[19] Kamal SM, Dixit US. Feasibility study of thermal autofrettage of thick-walled cylinders. ASME J Press Vessel Technol 2015;137(6):061207-1–061207-18.
[20] Kamal SM, Borsaikia AC, Dixit US. Experimental assessment of residual stresses induced by the thermal autofrettage of thick-walled cylinders. J Strain Anal Eng Des 2016;51(2):144–60.
[21] Dixit PM, Dixit US. Modeling of metal forming and machining processes: by finite element and soft computing methods. London: Springer; 2008.
[22] Chakrabarty J. Theory of plasticity. 3rd ed. Burlington: Butterworth-Heinemann; 2006.
[23] Noda N, Hetnarski RB, Tanigawa Y. Thermal stresses. 2nd ed. New York: Taylor and Francis; 2003.
[24] Zhu XK, Chao YJ. Effects of temperature-dependent material properties on welding simulation. Comput Struct 2002;80:967–76.
[25] ABAQUS User's Manual, Version 6.7, Dassault Systèmes Simulia Corp., Providence, RI, USA, 2007.